surfaces

MDPI

Article

Study on the Thermal Control Performance of Mg-Li Alloy Micro-Arc Oxidation Coating in High-Temperature Environments

Wentao Zhang [1,2], Shigang Xin [1,*], Qing Huang [1] and Haiyang Jiao [1]

[1] Shanghai Institute of Ceramics, Chinese Academy of Sciences, Shanghai 200050, China; zhangwentao27@163.com (W.Z.); huangqing@mail.sic.ac.cn (Q.H.); jiaohaiyang@mail.sic.ac.cn (H.J.)
[2] School of Materials and Chemistry, University of Shanghai for Science and Technology, Shanghai 200093, China
* Correspondence: sgxin@mail.sic.ac.cn

Abstract: This paper reports on the successful preparation of a low absorption–emission thermal control coating on the surface of LAZ933 magnesium–lithium alloy using the micro-arc oxidation method. This study analyzed the microstructure, phase composition, and thermal control properties of the coating using Scanning Electron Microscopy (SEM), X-ray diffraction (XRD), UV–visible near-infrared spectroscopy (UV-VIS-NIR) and infrared emissivity measurements. The results indicate that the hemispherical emissivity of the coating remains unaffected with an increase in temperature and holding time, while the solar absorption ratio gradually increases. The thermal control performance of the coating after a high-temperature experiment was found to be related to the diffusion of the Li metal element in the magnesium lithium alloy matrix, as determined by X-ray photoelectron spectroscopy (XPS), flame graphite furnace atomic absorption spectrometry (GFAAS) and Glow Discharge Optical Emission Spectroscopy (GD-OES). As the holding time is extended, the coating structure gradually loosens under thermal stress. The Li metal element in the substrate diffuses outward and reacts with O_2, H_2O and CO_2 in the air, forming LiO_2, LiOH, Li_2CO_3 and other products. This reaction affects the coating's solar absorption ratio in the end.

Keywords: Mg-Li alloy; micro-arc oxidation; thermal control coating

Citation: Zhang, W.; Xin, S.; Huang, Q.; Jiao, H. Study on the Thermal Control Performance of Mg-Li Alloy Micro-Arc Oxidation Coating in High-Temperature Environments. *Surfaces* **2024**, *7*, 969–978. https://doi.org/10.3390/surfaces7040063

Academic Editor: Aleksey Yerokhin

Received: 17 July 2024
Revised: 11 September 2024
Accepted: 29 October 2024
Published: 8 November 2024

1. Introduction

The density of magnesium–lithium alloys ranges from 1.35 to 1.65 g/cm^3, making it the lightest metal material [1]. It has attracted significant attention in the aerospace industry due to its potential for reducing spacecraft weight and advancing deep space exploration technology [2,3]. However, the high chemical activity of magnesium and lithium restricts the application of Mg-Li alloys [4–6]; surface treatment can enhance the corrosion resistance and provide new functions for the surface of Mg-li alloys. Common surface treatment methods for magnesium and its alloys include chemical conversion [7], electrochemical deposition [8], anodic oxidation [9] and micro-arc oxidation [10]. Micro-arc oxidation technology (MAO) stands out due to its environmentally friendly electrolytes' ability to directly grow ceramic coatings with excellent properties in situ, which has made it a popular choice for magnesium and its alloys [11–13].

The hemispherical emissivity of the magnesium–lithium alloy itself is approximately 0.1 with a solar absorption ratio of around 0.5. The surface temperature can reach hundreds of degrees Celsius when exposed to sunlight in space. Therefore, in aerospace applications, the coating on the surface of magnesium lithium alloys must have high corrosion resistance and have thermal control performance. The current research primarily focuses on creating thermal control coatings on Mg-Al alloys [14,15] by the MAO process. However, research on thermal control coatings for Mg-Li alloys is limited. Previous thermal control coatings on Mg-Li alloys [16–18] mostly focused on the influence of relevant process parameters on the thermal control performance of the coatings, without studying the change in thermal

control performance of the coatings in high-temperature environments. The lunar exploration project faces a significant challenge in the form of extreme surface temperatures ranging from −180 to +130 °C [19], which poses a great test for the high-temperature resistance of the thermal control coating. However, research on the structural changes in Mg-Li alloys in high-temperature environments mainly focuses on rolling [20,21] and hot compression experiments [22], and there is also a lack of research on the performance changes in Mg-Li alloy coatings at high temperatures. Therefore, it is crucial to analyze the properties and reasons for the thermal control coating on the surface of Mg-Li alloys in high-temperature environments.

This paper explores the microstructure and thermal control properties of the MAO thermal control coating applied to the surface of a Mg-Li alloy at elevated temperatures. The aim is to elucidate the mechanism of the effect of temperature on the performance of the coating and to provide a scientific basis for solving the problem of degradation thermal control performance in the application of Mg-Li alloy MAO thermal control coating.

2. Material and Methods

2.1. Preparation of MAO Coating

LAZ933 magnesium–lithium alloy was used as the base material, and the alloy material composition is shown in Table 1. The alloy plate was processed into 40 mm × 40 mm × 2 mm plate samples by wire cutting. After being polished with 200#, 400# and 1000# SiC sandpaper, the samples were ultrasonically cleaned in acetone for 10 min and dried. The experiment utilized deionized aqueous solutions of Na_2SiO_3 and KOH as electrolytes. The micro-arc oxidation process conditions are a Na_2SiO_3 concentration of 30 g/L; a KOH concentration of 1 g/L; PH kept at 11–12; a current density of 6 A/dm^2; a power supply frequency of 100 HZ; and a DC pulse power supply. The ceramic coating required for this process is prepared using multi-waveform programmed micro-arc oxidation pulse power supply equipment in the constant-current and limited-voltage power supply mode. The equipment consists of MAO power supply, an oxidation treatment tank and a water cooling system. A chiller was used for circulating cooling to maintain the electrolyte at a temperature between 20 and 40 °C. After the MAO process, the samples were cleaned with acetone and then dried in a blast drying oven.

Table 1. Chemical composition of LAZ933 magnesium–lithium alloy.

Element	Mg	Li	Al	Zn
%	BaL	8.5~9.5	2.5~3.5	2.5~3.5

2.2. High-Temperature Experiment

The prepared MAO coating of magnesium–lithium alloy was placed in an electric thermostatic air drying oven with two test pieces in each group, and the experiment was repeated three times. The first set of experimental conditions were as follows: the sample was placed in an electric thermostatic air drying oven for 24 h, and the temperature was set to 50 °C, 100 °C, 150 °C, and 200 °C, respectively; the second group of experimental conditions was set to 200 °C; and the sample was left for 0 H, 6 H, 12 H, 24 H, 48 H, 96 H, 144 H and 288 H, respectively, to analyze the impact of varying temperatures and holding durations on the composition and thermal radiation characteristics of the coating.

2.3. Performance Test and Tissue Observation

The phase composition of the coating was analyzed using the D2 PHASER X-ray (BRUKER AXS, Karlsruhe, Germany) diffractometer with a copper Ka target. The acceleration voltage and current were set to 40 KV and 150 mA, respectively, the scanning angle range was 10~80°, and the scanning rate was 10°/min. The reference card number in the database used for phase identification is 1557. The morphology of the coating was observed using a Magellan400 (FEI NanoPorts, Hillsboro, OR, USA) field emission

scanning electron microscope with an EDS spectrometer. The hemispherical emittance of the coating was measured using an AE1-RD1 (Aoptek, Beijing, China) infrared emittance measuring instrument. The solar absorption ratio of the coating was measured using a PE950 UV-VIS (PerkinElmer, Waltham, MA, USA) near-infrared spectrophotometer with a spectral measurement range of 250~2500 nm. The surface composition of the coating was detected using ESCALAB250Xi X-ray photoelectron spectroscopy (Thermo Fisher Scientific, Waltham, MA, USA). The excitation source used was an Al Ka ray, with a target power of 250 W and an X-ray incidence angle of 45°.The analytical model was a hemispherical model and the resulting data were corrected with C1s (284.8 eV). Element distribution along the coating depth was detected using glow discharge emission spectroscopy with a discharge voltage of 550 V and a gas pressure of 2 hPa. Ar of 1 vol%H_2 (purity 6.0) was used as the analytical gas for GD-OES analysis using the GD-Profiler 2 (HORIBA, Paris, France). After the high-temperature experiment, the test piece was ultrasonically cleaned in deionized water for 5 min and the deionized water content was 150 mL. The element content of the cleaned deionized water was tested using ZEEnit 700 P(Analytik Jena AG, Jena, Germany) flame graphite furnace atomic absorption spectrometry. All tests were performed at room temperature.

3. Results and Discussion

3.1. Thermal Radiation Performance Analysis

Table 2 presents the test results of the thermal control performance of the surface coating of the Mg-Li alloy after being held at different temperatures for 24 h. As the temperature increases, the hemispherical emissivity of the coating remains constant, whereas the solar absorption ratio of the coating increases with the temperature. When the temperature is 200 °C, the solar absorption ratio of the coating increases from 0.33 to 0.42 with the greatest degree of change.

Table 2. Test results of thermal control performance of MAO coatings after 24 h of treatment at different temperatures.

Temperature	Room Temperature	50 °C	100 °C	150 °C	200 °C
ε_H	0.89	0.89	0.89	0.89	0.89
α_S	0.33	0.35	0.36	0.38	0.42

Table 3 displays the changes in thermal radiation properties of the coating after different holding times. It can be seen that the hemispherical emissivity of the coating does not change with the extension of holding time, while the solar absorption ratio increases. Figure 1 shows the reflectance curve of the coating at various high temperatures. It can be found from Figure 1 that the reflectance curve of the coating decreases gradually with the holding time. Consequently, the degree of reflection of the coating towards the light also diminishes, indicating an increase in the absorption rate of the film layer. This result is consistent with the thermal control performance test of the coating after different holding times.

Table 3. Test results of thermal control performance of MAO coating at different holding times at 200 °C.

Time	0 h	6 h	12 h	24 h	48 h	96 h	144 h	288 h
ε_H	0.89	0.89	0.89	0.89	0.89	0.89	0.89	0.89
α_S	0.33	0.35	0.41	0.42	0.46	0.47	0.47	0.48

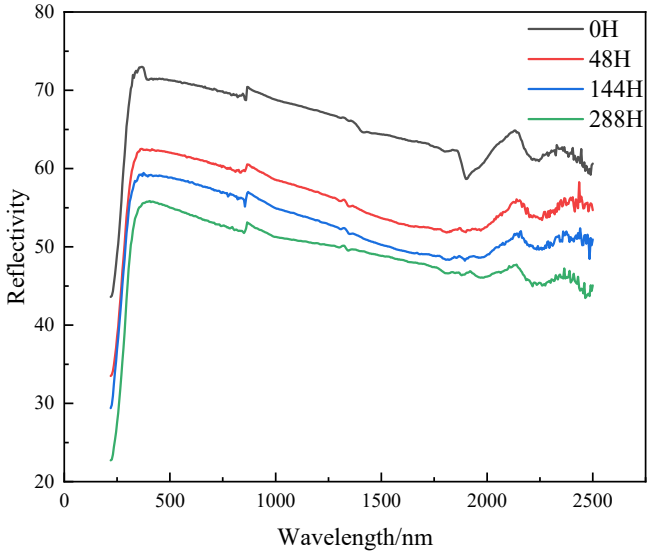

Figure 1. Reflectance curves of the coating after different holding times.

3.2. Analysis of Structure and Composition

Figure 2 shows the XRD patterns of the coating after different durations of high-temperature exposure. The phase compositions of the coating were MgO, Li_3Mg_7, and Mg_2SiO_4, respectively. The identified crystalline phases are described separately according to card numbers 71-1176 (PAN-ICSD), 65-6742 (PAN-ICSD), and 87-0061 (PAN-ICSD). The crystallinity of the coating after different insulation times was obtained through fitting analysis using Jade software, the values of which were 18.4%, 38.45%, 20.46% and 16.95%, respectively. This indicates that the crystallinity of the coating increases first and then decreases with time in a high-temperature environment. From Figure 2, it can be seen that the phase composition of the coating has not changed, indicating that the duration of high temperature has an impact on crystal growth and has a relatively small effect on phase composition.

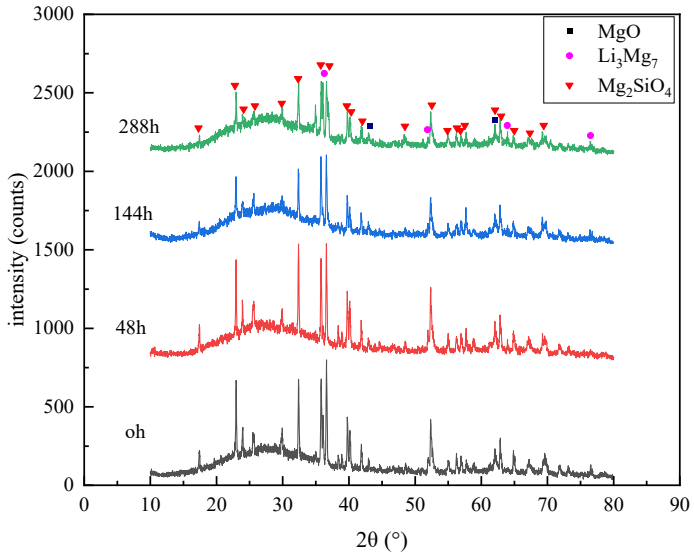

Figure 2. XRD spectra of coatings after different times at 200 °C.

Figure 3 shows the SEM surface morphology results, indicating an increase in the number of protrusions on the surface of the film layer with longer holding times. The micro-arc oxide film's porous structure allows for oxygen diffusion in high-temperature oxidation

environments leading to grain oxidation near the holes and an increase in protrusions on the coating's surface.

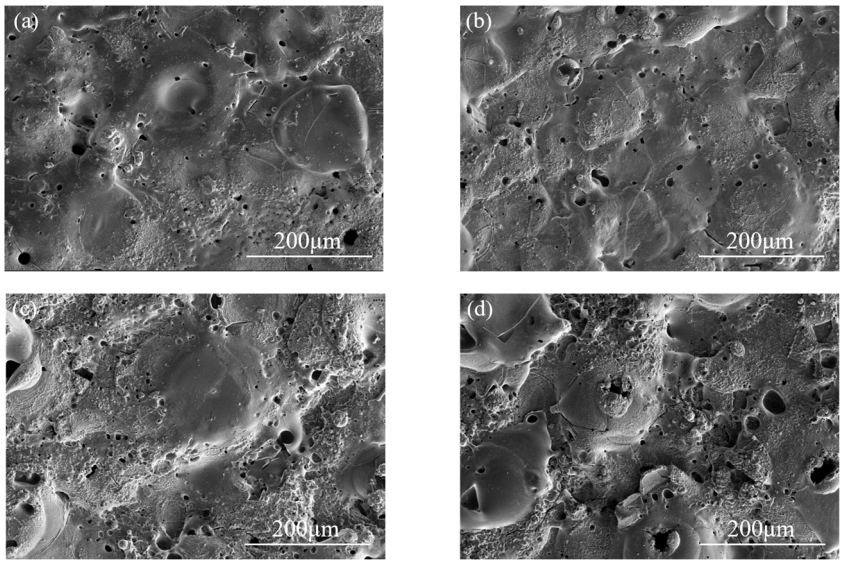

Figure 3. Surface topographies of the coatings after different high-temperature exposure times: (**a**) following 0 h of high temperature, (**b**) following 48 h of high temperature, (**c**) following 144 h of high temperature, and (**d**) following 288 h of high temperature.

Figure 4 shows the cross-section morphology of the coating after different holding times. It is found that as the holding time increases, the crack size in the coating increases. This phenomenon is related to the thermal stress generated under high-temperature environments. Simultaneously, the structure of the coating loosens gradually, enhancing its sunlight absorption capacity and resulting in an increase in the solar absorption ratio of the coating.

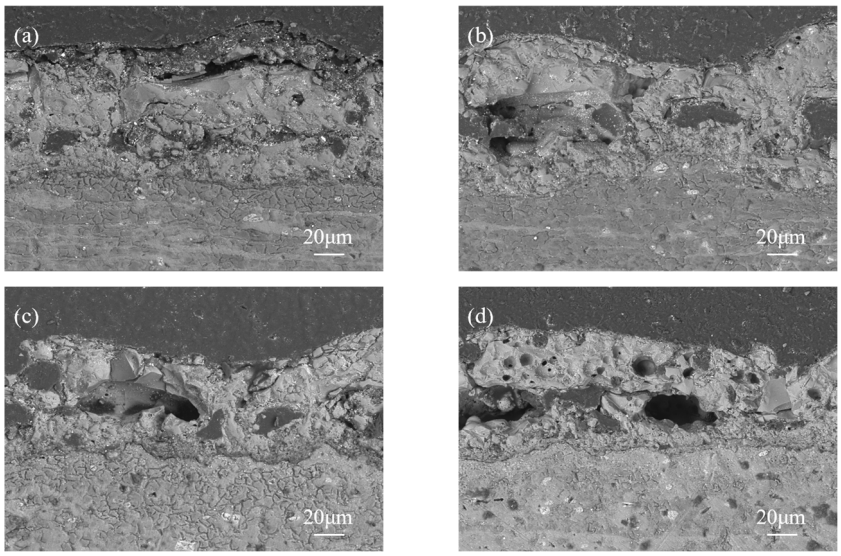

Figure 4. Cross-sectional topography of the coating after different high-temperature exposure times: (**a**) following 0 h of high temperature, (**b**) following 48 h of high temperature, (**c**) following 144 h of high temperature, and (**d**) following 288 h of high temperature.

3.3. XPS Analysis

XPS analysis was conducted on the coatings subjected to high-temperature treatments for different durations to study their chemical composition in detail. The chemical states

of Si, O, Mg and Li were studied. The results are shown in Figure 5. The Mg 1 s peak can be separated into two peaks: the peak at 1303.8 eV is from MgO and the other peak at 1304.2 eV is Mg_2SiO_4 [23]. The Si 2p peak is composed of two components, attributed to spin–orbit splitting, with combined energies of 102.30 and 102.95 eV, also indicating the presence of Mg_2SiO_4 [24]. The spectrum of O1s shows three oxygen molecules, where the peak at 530.3 eV is attributed to the typical metal–oxygen bond of MgO [25], while the peak at 531.2 eV corresponds to Mg_2SiO_4 [26]. The peak at 532.6 eV may be due to oxygen adsorbed on the surface of the coating [27]. In the Li1s spectrum, the peak at 55.40 ev is attributed to Li_2CO_3 [28]. The peak at 54.70 ev is LiOH [29]. It is found that the peak strength changes significantly with the extension of holding time, with the peak intensity of Li_2CO_3 and LiOH gradually increasing. This indicates that the high-temperature process may be accompanied by the diffusion of the Li element and the formation of Li_2O on the surface, and Li_2O is unstable and easily reacts with CO_2 to produce Li_2CO_3 in high-temperature environments. LiOH may form when Li_2O reacts with water vapor in the air after the coating leaves the high-temperature environment.

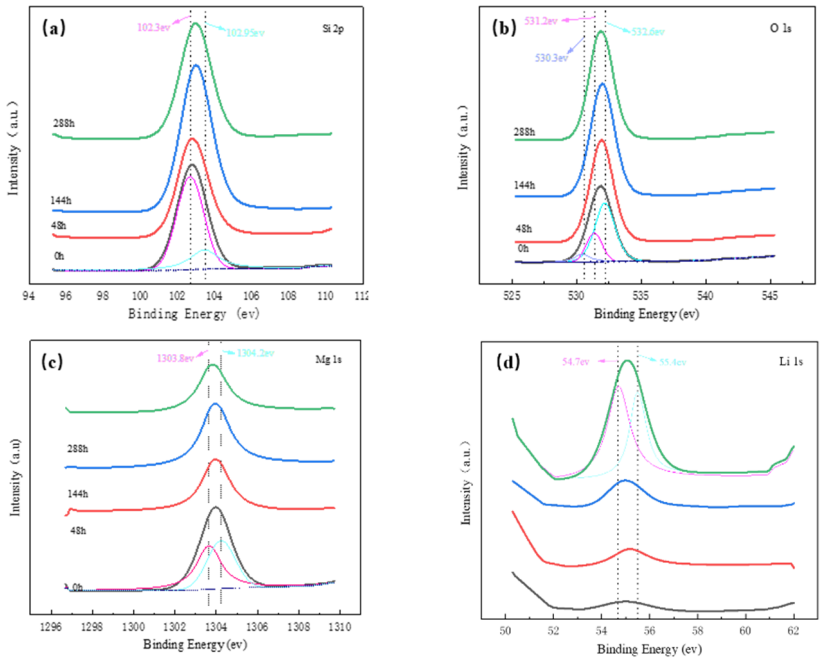

Figure 5. XPS spectra of the coating after different high-temperature exposure times: (**a**) Si 2p, (**b**) O 1s, (**c**) Mg 1s, and (**d**) Li 1s.

Table 4 shows the element content analysis of XPS. It can be seen that with the increase in the high-temperature exposure time, contents of Mg, Al and Zn in the matrix elements do not change significantly, while the content of the Li element increases significantly with the extension of holding time.

Table 4. Elemental content analysis of XPS.

Atomic %	0 h	48 h	144 h	288 h
Mg1s	3.44	3.74	3.45	3.77
Li1s	14.71	16.35	18.15	22.24
Al2p	4.04	3.43	3.60	3.53
Zn2p	1.33	1.09	1.14	1.17

3.4. Atomic Absorption Spectrometry

Under high-temperature conditions, the internal metal ions are more likely to diffuse out of the micro-arc oxide layer and be oxidized. In order to verify whether there is element diffusion inside the alloy on the coating surface, test pieces that have not been treated at high temperature and samples processed at 200 °C for different amounts of time are put into deionized water for ultrasonic cleaning. The deionized water after cleaning was tested by atomic absorption spectrometry. Table 5 shows the change in the solar absorption ratio of the coating before and after cleaning. It can be found that the solar absorption ratio of the coating decreases slightly after ultrasonic cleaning with deionized water.

Table 5. Solar absorption ratio of the coating before and after ultrasonic cleaning.

	0 h	**48 h**	**144 h**	**288 h**
α_S (Before cleaning)	0.33	0.46	0.47	0.48
α_S (After cleaning)	0.33	0.43	0.44	0.46

Table 6 shows the test results of atomic absorption spectrometry. It can be seen that contents of Mg, Al and Zn ions do not change significantly with the extension of holding time at 200 °C, while the content of Li ions in deionized water gradually increases. This result shows that during the high-temperature process, diffusion of the Li metal element in the alloy from the matrix to the coating occurs. During the diffusion of Li-ions to the coating, they easily react with O_2, H_2O and CO_2 in the air to form LiO_2, LiOH, Li_2CO_3 and other products, which deepens the color of the coating surface. In the process of ultrasonic cleaning in deionized water, these products dissolve in the deionized water, increasing the Li element content. However, the dissolution of these reaction products leads to a decrease in the solar absorption ratio of the coating. Therefore, the diffusion of Li metal ions may be one of the reasons for the increase in the solar absorption ratio of the coating.

Table 6. Atomic absorption spectroscopy test results.

Components Analyzed (μg/mL)	**Deionized Water**	**0 h**	**48 h**	**144 h**	**288 h**
Mg	0.28	0.32	0.35	0.37	0.31
Li	<0.004	1.76	14.25	19.04	29.46
Al	0.06	0.04	0.05	0.06	0.04
Zn	<0.002	0.01	0.01	0.01	0.01

3.5. GD-OES Analysis

The distribution of coating elements at high temperature was studied by the GD-OES method. The depth profile analysis of the coating before and after exposure to high temperature for 288 h was carried out, and the results are shown in Figure 6.

As can be seen from Figure 6, the contents of Mg, Al and Zn in the coating did not change before and after high-temperature treatment, while the strength of the Li element increased significantly after high-temperature treatment. This indicates that the Li element in the substrate diffuses into the coating in high-temperature environments, which is also consistent with previous experimental findings.

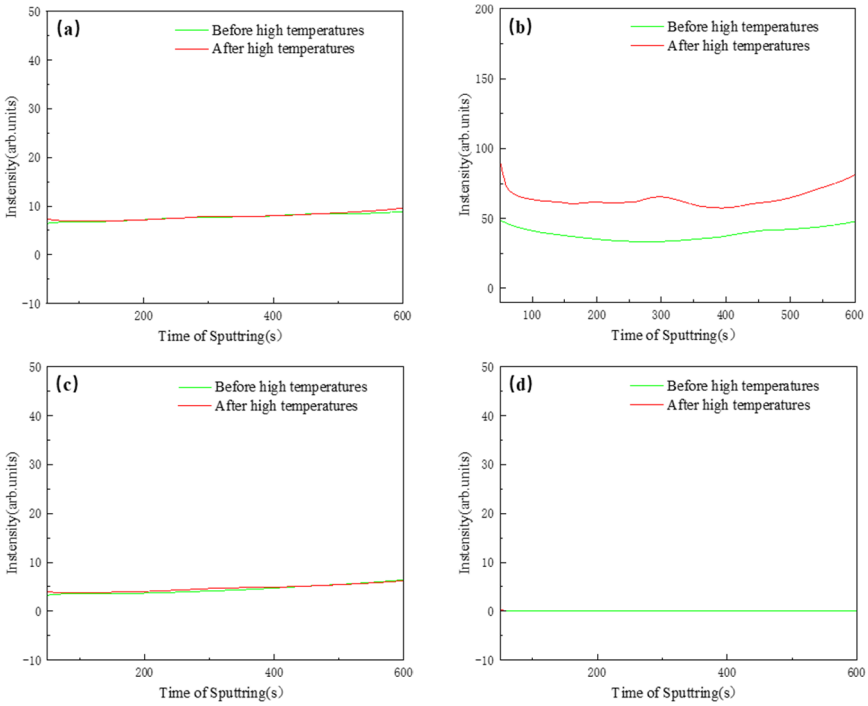

Figure 6. Spectral test spectrum of glow power generation: (**a**) Mg, (**b**) Li, (**c**) Al, and (**d**) Zn.

4. Conclusions

Experimental analysis was conducted on the performance changes of micro-arc oxidation thermal control coating on a magnesium–lithium alloy under a high-temperature environment, and the following conclusions were drawn:

1. The solar absorption rate of the coating gradually increases with temperature and high-temperature exposure time, while the hemispherical emissivity remains unchanged.

2. As the high-temperature exposure time increases, the porous structure of the micro-arc oxidation coating becomes loose under the influence of thermal stress, leading to a gradual increase in the size of pores and cracks. Due to the small volume parameter of lithium element, when the structure of the coating is loose, lithium element is more likely to diffuse outward from the substrate, react with O2, H2O, and CO2 in the air on the surface of the coating, and generate reaction products such as Li2CO3 and LiOH. These reaction products have a high absorption rate of light energy, resulting in an increase in the solar absorption rate of the coating.

The study on the thermal control performance changes of micro-arc oxidation thermal control coatings on magnesium lithium alloys under a high-temperature environment lays the foundation for the subsequent application of magnesium lithium alloys in aerospace, which is beneficial for the development of such alloys in thermal control coatings.

Author Contributions: Conceptualization, S.X. and W.Z.; methodology, S.X. and W.Z.; software, W.Z.; validation, S.X. and W.Z.; formal analysis, S.X. and W.Z.; investigation, W.Z. and Q.H.; resources, S.X. and Q.H.; data curation, S.X. and W.Z.; writing—original draft preparation, W.Z. and S.X.; writing—review and editing, H.J.; visualization, H.J. and Q.H.; supervision, S.X.; project administration, S.X.; funding acquisition, S.X. All authors have read and agreed to the published version of the manuscript.

Funding: This research received no external funding.

Data Availability Statement: The authors confirm that the data supporting the findings of this study are available within the article.

Conflicts of Interest: The authors declare no conflict of interest.

References

1. Yang, L.H.; Li, J.Q.; Zheng, Y.L.; Jiang, W.; Zhang, M. Electroless Ni-P plating with molybdate pretreatment on Mg-8Li alloy. *J. Alloys Compd.* **2009**, *467*, 562–566. [CrossRef]
2. Tang, H.; Yan, Y.D.; Zhang, M.L.; Li, X.; Han, W.; Xue, Y.; Zhang, Z.J.; He, H. Fabrication of Mg–Pr and Mg–Li–Pr alloys by electrochemical co-reduction from their molten chlorides. *Electrochim. Acta* **2013**, *107*, 209–215. [CrossRef]
3. O'Connor, A.; Park, C.; Baciak, J.E.; Manuel, M.V. Mitigating space radiation using magnesium(-lithium) and boron carbide composites. *Acta Astronaut.* **2024**, *216*, 37–43. [CrossRef]
4. Jiang, B.; Zhang, C.; Wang, T.; Qu, Z.; Wu, R.; Zhang, M. Creep behaviors of Mg–5Li–3Al–(0,1)Ca alloys. *Mater. Des.* **2012**, *34*, 863–866. [CrossRef]
5. Li, C.Q.; Xu, D.K.; Zhang, Z.R.; Han, E.H. Influence of the lithium content on the negative difference effect of Mg-Li alloys. *J. Mater. Sci. Technol.* **2020**, *57*, 138–145. [CrossRef]
6. Song, D.; Ma, A.B.; Jiang, J.H.; Lin, P.H.; Yang, D.H.; Fan, J.F. Corrosion behaviour of bulk ultra-fine grained AZ91D magnesium alloy fabricated by equal-channel angular pressing. *Corros. Sci.* **2011**, *53*, 362–373. [CrossRef]
7. Zhang, J.M.; Hou, A.R.; Li, J.C.; Lian, D.D.; Zhang, M.C.; Wang, Z.H. Enhanced Corrosion and Wear Resistance of LA43M Magnesium-Lithium Alloy with Magnesium-Aluminum Layered Double Hydroxide Coating. *J. Mater. Eng. Perform.* **2023**, *32*, 3550–3562. [CrossRef]
8. Ouyang, Y.; Chen, Z.; Guo, E.; Qiu, R.; Wang, X.; Kang, H.; Wang, T. Bioinspired superhydrophobic surface via one-step electrodeposition and its corrosion inhibition for Mg-Li alloy. *Colloids Surf. A Physicochem. Eng. Asp.* **2022**, *648*, 129145. [CrossRef]
9. Liu, Y.Y.; Li, J.F.; Zhang, L.G.; Chen, X.C.; Bai, J.Y.; Cui, Q.X. Preparation and properties of anodizing thermal control coating on magnesium-lithium alloy surface. *J. Aeronaut. Mater.* **2018**, *38*, 36–42.
10. Ma, X.C.; Jin, S.; Wu, R.; Ji, Q.; Hou, L.; Krit, B.; Betsofen, S. Influence alloying elements of Al and Y in Mg Li alloy on the corrosion behavior and wear resistance of MAO coatings. *Surf. Coat. Technol.* **2022**, *432*, 128042. [CrossRef]
11. Chen, Y.H.; Liang, W.U.; Yao, W.H.; Chen, Y.N.; Wu, J.H.; Yuan, Y.; Jiang, B.; Atrens, A.; Pan, F.S. Synthesis of ZIF-67 film in micro-arc oxidation anticorrosion coating on AZ31 magnesium alloy. *Trans. Nonferrous Met. Soc. China* **2023**, *33*, 2631–2645. [CrossRef]
12. Liu, R.; Liu, Y.; Yong, Q.; Xie, Z.H.; Wu, L.; Zhong, C.J. Highly corrosion-resistant ZIF-8-integrated micro-arc oxidation coating on Mg alloy. *Surf. Coat. Technol.* **2023**, *463*, 129505. [CrossRef]
13. Xiong, Y.; Yu, Y.; Yang, J. Fatigue behavior after pre-corroded in a simulated body fluid for ZK60 magnesium alloy prepared by micro-arc oxidation. *Fatigue Fract. Eng. Mater. Struct.* **2022**, *45*, 239–258. [CrossRef]
14. Wang, X.; Lu, X.; Ju, P.; Chen, Y.; Zhang, T.; Wang, F. Thermal control property and corrosion resistance of PEO coatings on AZ91 Mg alloy. *Surf. Coat. Technol.* **2020**, *139*, 125709. [CrossRef]
15. Zhang, Z.; He, F.; Huang, C.; Song, Z.; Yang, J.; Wang, X. Effect of Fe^{3+} and F^{-} on black micro-arc oxidation ceramic coating of magnesium alloy. *Int. J. Appl. Ceram. Technol.* **2022**, *19*, 2203–2212. [CrossRef]
16. Yao, Z.; Xia, Q.; Ju, P.; Wang, J.; Su, P.; Li, D.; Jiang, Z. Investigation of absorptance and emissivity of thermal control coatings on Mg–Li alloys and OES analysis during PEO process. *Sci. Rep.* **2016**, *6*, 29563. [CrossRef]
17. Xia, Q.; Zhang, D.; Li, D.; Jiang, Z.; Yao, Z. Preparation of the plasma electrolytic oxidation coating on MgeLi alloy and its thermal control performance. *Surf. Coat. Technol.* **2019**, *369*, 252–256. [CrossRef]
18. Wu, G.; Zhao, D.; Lin, X.; Liu, J.; Ji, X. Investigation of an environmentally friendly coloring coating for magnesium-lithium alloy micro-arc oxidation. *Surf. Interfaces* **2020**, *20*, 100513. [CrossRef]
19. Bauch, K.E.; Hiesinger, H.; Helbert, J.; Robinson, M.S.; Scholten, F. Estimation of lunar surface temperatures and thermophysical properties: Test of a thermal model in preparation of the MERTIS experiment onboard BepiColombo. *Planet. Space Sci.* **2014**, *101*, 27–36. [CrossRef]
20. Li, X.; Guo, F.; Ma, Y.; Jiang, L.; Lai, H.; Liu, H.; Zhang, D.; Pei, R. Rolling texture development in a dual-phase Mg-Li alloy: The role of temperature. *J. Magnes. Alloys* **2023**, *11*, 2980–2990. [CrossRef]
21. Li, X.; Jiang, L.; Guo, F.; Ma, Y.; Yu, H.; Chen, Q.; Liu, H.; Zhang, D. Unveiling the rolling texture variations of α-Mg phases in a dual-phase Mg-Li alloy. *J. Magnes. Alloys* **2024**, *12*, 2557–2568. [CrossRef]
22. Król, M.; Snopiński, P.; Pagáč, M.; Hajnyš, J.; Petrů, J. Hot Deformation Treatment of Grain-Modified Mg–Li Alloy. *Materials* **2020**, *13*, 4557. [CrossRef] [PubMed]
23. Gao, H.; Zhang, M.; Yang, X.; Huang, P.; Xu, K. Effect of Na_2SiO_3 solution concentration of micro-arc oxidation process on lap-shear strength of adhesive bonded magnesium alloys. *Appl. Surf. Sci.* **2014**, *314*, 447–452. [CrossRef]
24. Brambilla, R.; Radtke, C.; Dos Santos, J.H.; Miranda, M.S. An investigation on structure and texture of silica-magnesia xerogels. *J. Sol-Gel Sci. Technol.* **2009**, *51*, 70–77. [CrossRef]
25. Moon, S.H.; Heo, T.W.; Park, S.Y.; Kim, J.H.; Kim, H.J. The effect of the dehydration of Mgo films on their XPS spectra and electrical properties. *J. Electrochem. Soc.* **2007**, *154*, 408–412. [CrossRef]
26. Seyama, H.; Soma, M. Bonding-state characterization of the constitutent elements of silicate minerals by X-ray photoelectron spectroscopy. *J. Chem. Soc.* **1985**, *81*, 485–495. [CrossRef]
27. Liang, H.; Lin, J.; Jia, H.; Chen, S.; Qi, J.; Cao, J.; Lin, T.; Feng, J. Hierarchical NiCo-LDH@NiOOH core-shell heterostructure on carbon fiber cloth as battery-like electrode for supercapacitor. *J. Sol-Gel Sci. Technol.* **2018**, *378*, 248–254. [CrossRef]

28. Zhao, B.; Li, J.; Guillaume, M.; Dendooven, J.; Detavernier, C. In vacuo XPS investigation of surface engineering for lithium metal anodes with plasma treatment. *J. Energy Chem.* **2022**, *66*, 295–305. [CrossRef]
29. Kozen, A.C.; Pearse, A.J.; Lin, C.F.; Schroeder, M.A.; Noked, M.; Lee, S.B.; Rubloff, G.W. Atomic Layer Deposition and in Situ Characterization of Ultraclean Lithium Oxide and Lithium Hydroxide. *J. Phys. Chem. C* **2014**, *118*, 2774. [CrossRef]